Tomographic Biomarkers Predicting Progression to Fibrosis in Treated Neovascular Age-Related Macular Degeneration: A Multimodal Imaging Study

Giuseppe Casalino, MD, FEBO,[1,2] Michael R. Stevenson, MSc,[1] Francesco Bandello, MD, FEBO,[2] Usha Chakravarthy, MD, PhD[1]

Purpose: To describe the photoreceptor—retinal pigment epithelium (RPE) interface changes and to analyze the relationships between these features and hyperreflective material (HRM) with scarring and atrophy at the macula of patients with neovascular age-related macular degeneration (nAMD).

Design: Retrospective single-center observational study.

Participants: A total of 150 eyes from 144 patients with naive nAMD were included.

Methods: All patients had OCT (HRA-OCT Spectralis, Heidelberg Engineering, Heidelberg, Germany) at baseline and at 1, 3, 6, and 12 months. Macular scar and macular atrophy (MA) were determined on multimodal imaging, including color fundus (CF) and near-infrared imaging at baseline and month 12 (M12).

Main Outcome Measures: Change in HRM type (undefined and well-defined) and location, development of fibrotic or nonfibrotic macular scar, MA, and best-corrected visual acuity (BCVA) at M12.

Results: At baseline, eyes with fibrin on CF had thicker and wider HRM on OCT that correlated strongly with presence of undefined HRM. The proportion of eyes with undefined HRM fell dramatically by month 1 but well-defined HRM increased. At M12 defined HRM was strongly associated with macular scar (chi-square, 82.1; $P < 0.001$). Ordinal regression showed that both the thickness and the width of HRM were significant risk factors for development of fibrotic scar ($P < 0.001$ and $P = 0.02$) but not nonfibrotic scars ($P = 0.67$ and $P = 0.65$). Fibrotic macular scar ($P = 0.001$) but not nonfibrotic scar ($P = 0.129$) negatively affected visual acuity at M12. Ordinal regression showed that the risk factors for progression to MA were reticular pseudodrusen and thinner HRM ($P = 0.017$ and $P = 0.028$, respectively). MA negatively affected BCVA at M12 ($P < 0.001$).

Conclusion: Our study supports the role of HRM as an important biomarker for the evolution of macular scar and atrophy in patients with nAMD undergoing treatment with anti-VEGF therapies. Undefined HRM can resolve with treatment, whereas well-defined HRM likely contains vascular complexes and fibrotic elements. *Ophthalmology Retina 2017;■:1—11 © 2017 by the American Academy of Ophthalmology. This is an open access article under the CC BY-NC-ND license (*http://creativecommons.org/licenses/by-nc-nd/4.0/*).*

Supplemental material is available at www.ophthalmologyretina.org.

Choroidal neovascularization (CNV) at the macula of patients with age-related macular degeneration (AMD) can lead to severe vision loss in more than 40% of patients by 3 years if left untreated.[1] Scarring and atrophy at the macula negatively affect the natural history of untreated neovascular AMD (nAMD).[2]

Although the widespread use of intravitreal anti−vascular endothelial growth factor (anti-VEGF) treatment has substantially improved the long-term prognosis of nAMD,[3] retinal scarring and atrophy have been identified as predictors of vision loss even in patients with nAMD who have been treated with anti-VEGF therapies.[3−5]

Subretinal hyperreflective material is an optical coherence tomography (OCT) finding in nAMD that has been found to correlate with fluorescein angiography (FA) leakage in eyes with active CNVs,[6] especially with subretinal (SR) CNVs.[7] In the Comparison of Age-related macular degeneration Treatments Trials (CATT) study, the presence of SR hyperreflective material on OCT was found to correlate with retinal scar development after treatment.[8] Because we recently showed that this material can be located in compartments other than SR, we preferred to use the term *hyperreflective material* (HRM).[9] We observed that when HRM is undefined and subretinally

located, it strongly correlates with the presence of fibrin exudation seen on color photography before initiation of treatment.[9] We also observed that the characteristics of the change in HRM over time during anti-VEGF treatment became more defined and located mostly in the subretinal pigment epithelium (sub-RPE) compartment, suggesting evolution into scar tissue.[9] With upcoming treatment modalities targeting fibroblast proliferation and with potential to limit scarring,[10] there has been increasing interest for the early detection of biomarkers of fibrosis on tomography.[11] Notably, associations between newly recognized OCT features and retinal scar evolution have been described.[12]

A systematic analysis including novel OCT biomarkers and macular scar and atrophy has not been performed and may clarify the pathophysiology of these events over time in eyes treated with anti-VEGF.

The goals of our study were (1) to describe in detail the morphologic alterations over time at the photoreceptor−RPE interface in the different neovascular AMD subtypes; (2) to study the development of HRM type, presence, location, and macular scar and atrophy evolution; and (3) to explore relationships with visual acuity (VA) over time in eyes treated with anti-VEGF.

Methods

Design

This was a retrospective analysis using data from electronic medical care records and associated imaging repositories of patients seen in a single tertiary referral eye care center. The institutional review board of Belfast Trust determined that approval was not required for this study because it contains findings from an aggregated analysis of functional and imaging data and no patient identifiers are included.

Population and Study Protocol

We identified 1671 new patients in the electronic medical care records who were patients at the retina clinics at the Belfast Health and Social Care Trust between January 2012 and April 2014. Our hypothesis was that HRM composition and location would differ by nAMD subtype. To ensure sufficient representation of these categories, we prespecified a sample of 150 eyes because previous experience[9] suggested that we would expect around 35 to 40 eyes of type 1 and type 2 nAMD, a similar proportion of mixed (types 1 and 2), some 25 retinal angiomatous proliferation and 15 cases of polypoidal choroidal vasculopathy (PCV). After exclusion of other diagnoses, we selected 144 consecutive patients, 6 of whom had bilateral presentation and all of whom had confirmed neovascular AMD, yielding a total of 150 eyes eligible for inclusion. For eligibility, we specified the following: (1) commencement of treatment with an anti-VEGF; (2) follow-up of at least 12 months; (3) CF imaging performed at baseline and month 12 (M12); (4) OCT imaging performed at baseline and at months 1, 3, 6, and 12; and (5) FA and indocyanine green angiography performed at baseline for purposes of nAMD classification. CF imaging was performed on the Visucam Pro NM (Carl Zeiss Meditec AG, Jena, Germany) or as multicolor (MC) scanning laser imaging on the Heidelberg system (Heidelberg Retinal Angiograph, Heidelberg Engineering, Heidelberg, Germany). Optical coherence tomography, near-infrared (NIR), fundus autofluorescence, FA,

and indocyanine green angiography were performed in all patients on the Heidelberg system. The OCT scan protocol included 37-line raster scans (20 × 15 degrees) consisting of 512 A-scans for every line. The "follow-up" mode of the eyetracking-assisted system (AutoRescan, Heidelberg Spectralis) was used during the follow-up visits.

There were no visual acuity (VA) eligibility criteria.

The study patients had treatment with either ranibizumab or aflibercept and received a loading dose of 3 injections given monthly. On completion of the loading phase, patients receiving ranibizumab were retreated using as-needed criteria[13]: evidence of new retinal hemorrhage, or recurrence or persistence of intraretinal (IR) or SR fluid on OCT. Those receiving aflibercept were on a fixed regimen of bimonthly injections for 1 year.[14]

Grading

We graded for presence of fibrin, blood, and lipid using CF and/or MC without reference to any other imaging modality. Subsequent to this grading, all other gradings were performed using a multimodal approach. At baseline, fundus autofluorescence was graded to rule out the presence of hyper-autofluorescent signal suggestive of vitelliform material, which represented a criterion of exclusion.

Fluorescein angiography and indocyanine green angiography images were graded to determine the type of nAMD using the definitions provided by a multimodal imaging classification,[15] after which the eyes were classified as occult (type I); classic (type II); retinal angiomatous proliferation (type III); mixed (with classic and occult component); and polypoidal choroidal vasculopathy (PCV).

We next delineated areas of macular scarring and atrophy using all available imaging modalities. Macular scar and atrophy were graded using the following definitions. MA was defined as a single or multiple areas of hypopigmentation with well-defined borders and visible large choroidal vessels on CF that corresponded to window defects on angiography and/or to the loss of cellular layers (outer retina, RPE, and choriocapillaris) on the accompanying tomograms.

Macular scar identification was based on both color and fluorescein characteristics. On CF or MC, scar was said to be present if there were well-delineated areas of yellow-white tissue with corresponding initial hypofluorescence, with late hyperfluorescence and staining on fluorescein angiograms. Lesions were further categorized as showing fibrotic and nonfibrotic scars using definitions identical to those of the CATT study.[16]

At M12, retinal angiography was not available on the vast majority of eyes; therefore we graded for the presence of scar and MA on CF, MC, and/or near-infrared imaging.

A graded categorical approach was used to determine the extent of fibrotic and nonfibrotic scarring: no scar; barely visible, for a scar involving approximately 25% of the lesion; mild, for a scar involving approximately 50% of the lesion; moderate, for a scar involving approximately 75% of the lesion; and severe, when the entire lesion consisted of a scar. A similar scoring system was applied to grade for MA (no atrophy, barely visible, mild, moderate, and severe when the entire lesion area was atrophic).

Optical coherence tomography images were generally available at all visits, but we chose to grade only those from baseline and from months 1, 3, 6, and M12 visits. We used the recently developed consensus for definitions on OCT nomenclature.[17] The RPE was defined as the hyperreflective band between the choriocapillaris and the interdigitation zone (this band is not normally separable from the Bruch membrane in the scans from the current generation of spectral-domain OCT and therefore is defined as the RPE−Bruch complex). The ellipsoid zone (EZ) was defined as the second hyperreflective band internal to the RPE. The external limiting membrane (ELM) was defined as a discrete

hyperreflective band at the outermost border of the outer nuclear layer and located internal to the EZ band.

We also graded for the presence of reticular pseudodrusen, which we defined as the hyperreflective deposits located at the level of the photoreceptor matrix outer retina, as this feature has been shown to be associated with a high risk of geographic atrophy.[18]

We examined all the scans of the macular raster for regions of abnormal hyperreflectivity and localized these to the IR, to the SR, or in the subretinal pigment epithelial (sub-RPE) compartments. We used the same definition described in our previous article[9] to distinguish between types of HRM. HRM with high reflectivity whose boundaries could be clearly delineated from the surrounding neural components of the retina was classified as well-defined. HRM with low reflectivity and whose borders were less well distinguishable from surrounding neural components was classified as undefined.

HRM was considered well-defined if all B scans of the raster showed a clear demarcation from neurosensory retinal elements. As the acquisition protocols in our clinics included capture on the rescan mode of the Heidelberg, this allowed the baseline and follow-up B scans to be aligned for comparison and permitted the grader to assign the eye to well-defined or undefined status at postbaseline visits.

Maximum HRM thickness and width were measured with the caliper provided by the Heidelberg Eye Explorer software (version 1.9.10.0; Heidelberg Engineering). HRM thickness was measured from the inner border of the HRM to the inner border of the Bruch membrane as described in the CATT study.[8] HRM width was measured as the maximum distance between the 2 sides of the HRM.

We looked for the presence of a "hyperreflective line above the HRM," which was defined as a band of hyperreflectivity with no continuity with any other visible hyperreflective bands. "RPE splitting" was defined as a splitting of the RPE on OCT into 2 distinct hyperreflective bands. RPE thickening was defined as a focal increased reflectivity of the outer retinal band corresponding to the RPE. An "enveloped HRM" was said to be present if the hyperreflective band attributable to the split RPE completely enclosed the HRM, as also described in a recent article.[19]

OCT scans were graded for the presence or absence of pigment epithelial detachment, subretinal fluid, and intraretinal fluid. Pigment epithelial detachment was graded as fibrovascular, serous, or irregular shallow RPE elevation. OCT was also graded for the presence of bridge arch–shaped serous retinal detachment (SRD), defined as subretinal fluid accumulation with a steep angle at the junction between the RPE and the sensory retina with adhesion areas between the sensory retina and the underlying HRM.[12]

At baseline and M12, OCT scans were also graded for presence of outer retinal tubulations[20] and cystoid macular degeneration (CMD).[21]

The scan with the maximum pathology was selected for grading of RPE, EZ, and ELM layer integrity. We defined maximum pathology as the scan with the maximum lesion thickness (neurosensory retina thickness including height of the pigment epithelial detachment, if present).

A graded categorical approach was used to determine the intactness of these layers, with a score of 0 (intact layer), 1 (25% disrupted), 2 (50% disrupted), 3 (75% disrupted), or 4 (completely disrupted).

The grading was performed by a single retina specialist (G.C.) with quality assurance carried out by 2 retina specialists (U.C. and F.B.).

Statistical Analysis

Data were analyzed using the Statistical Packages for Social Sciences (SPSS, Version 22, IBM Corp, Armonk, NY). Descriptive statistics were generated for continuous variables and categorical variables. We explored the relationship between best-corrected visual acuity (BCVA) with HRM type at baseline and M12 (no HRM, undefined HRM, and well-defined HRM). At M12, however, there were only 2 eyes with undefined HRM, so we did not compute means for this category of eyes at this visit. For the baseline comparison, we used an analysis of variance (ANOVA) with post hoc tests and at M12 a comparison of means using the *t* test.

We tested relationships between final BCVA and severity grades of MA by generating homogeneous subsets. To explore the relationship of BCVA with change in HRM status at M12, we used an ANOVA with BCVA at baseline as the covariate. We also performed a subanalysis of eyes with only undefined HRM at baseline and explored visual outcome by whether they developed well-defined HRM or not. We used linear regression to test relationships between BCVA and HRM thickness and width at baseline and M12 (cross-sectional models), and a longitudinal model to test change in BCVA versus change in HRM thickness and width, with BCVA at baseline as a fixed factor.

As the grading had generated an extensive list of variables (RPE splitting, RPE disruption, subretinal fluid, bridge sign, hyperreflective line over HRM, HRM type, disruption of the EZ, disruption of the ELM), all of which had been measured at multiple points in time (months 0, 1, 3, 6, and 12), we undertook exploratory analyses for each variable to identify only the specific time points that had a significant relationship with BCVA at M12. Our final regression model was performed with a stepwise forward elimination algorithm with only those variables that reached significance in the previous steps included as the explanatory variables.

Ordinal regression was used to examine predictors for the outcomes of scar and atrophy that had been graded on a categorical scale. To examine the effect of scar and atrophy on final VA, we used a general linear model with BCVA at M12 as the outcome variable, BCVA at baseline as the covariate, and scar or atrophy at M12 as the fixed factor (with atrophy treated as a nominal variable).

Results

Baseline Characteristics and HRM Changes

A total of 150 eyes from the 144 patients selected with active nAMD (6 with bilateral presentation) were included in the study. The mean patient age of the sample was 78.4±7.8 years (range, 53–97 years), and 96 were females.

Baseline and M12 BCVA and number of treatments given by nAMD subtypes are shown in Table 1. Mean BCVA was 57.63±14.34 ETDRS letters at baseline and 61.03±16.50 ETDRS letters at M12. On average, baseline BCVA was worst when any classic CNV was present (type 2 or mixed) and by M12 had improved in all nAMD groups with no statistically significant differences. The mean number of intravitreal injections performed during year 1 was 7.03±1.90 (range 3–11). One hundred thirty-seven eyes were treated with Ranibizumab, of which 8 with PCV had combination treatment with verteporfin photodynamic therapy, and 13 eyes were treated with aflibercept. No statistically significant differences were observed between the nAMD subtype groups for the number of intravitreal injections administered.

The proportion of eyes with no HRM, well-defined HRM, and undefined HRM by visit and location is shown in Table 2. Baseline and M12 HRM thickness and width by nAMD subtypes are shown in Table 3. The thickness and width of both undefined and well-defined HRM reduced over time (Figs 1 and 2), but

Table 1. Age, Number of Treatments, and Initial and Month 12 BCVA by Angiographic Subtype of Neovascular Age-Related Macular Degeneration

CNV	Age (yrs)	No. of Injections	Baseline BCVA	M12 BCVA	P Value
Type 1 (n = 40)	77.9±7.6	7.5±1.8	64.5±11.1	65.2±12.1	0.67
Type 2 (n = 41)	79.8±7.8	6.8±1.7	54.1±15.6	59.6±18.8	0.006
Type 3 (n = 31)	79.0±5.6	6.7±1.8	55.4±13.1	56.9±16.3	0.54
Mixed (n = 27)	78.0±7.6	6.8±1.8	53.3±14.1	57.4±18.2	0.16
PCV (n = 11)	74.5±12.4	7.4±2.9	62.2±15.8	71.4±11.3	0.005
Total (n = 150)	78.4±7.8	7.0±1.9	57.6±14.3	61.0±16.5	0.001

BCVA = best-corrected visual acuity; CNV = choroidal neovascularization; M12 = month 12; PCV = polypoidal choroidal vasculopathy.
BCVA is reported in ETDRS letters. P values were determined using paired t test.

proportionately greater reductions were observed with undefined HRM compared with well-defined HRM; these differences were highly significant on univariate analysis (Table 4).

Fibrin was present in 62.0% of eyes at baseline and was by far the most frequent component on CF for all the CNV subtypes, with the exception of the PCV subtype in which blood was the most frequent finding (Supplemental Table S1, available at www.ophthalmologyretina.org).

Eyes graded as exhibiting fibrin on the CF had thicker and wider HRM on the OCT grading (independent samples t test $P = 0.001$ and $P < 0.001$, respectively).

No relationship was detected between drug, dosing regimens, number of injections, and HRM morphology changes over time.

HRM and Visual Outcome

ANOVA with post hoc tests demonstrated the presence of a gradient in BCVA by HRM type at baseline, with the best VA observed in the group without HRM and the worst VA in the group with well-defined HRM (Table 4).

At M12, there were only 2 eyes with undefined HRM. Therefore the only comparison made was between eyes with well-defined HRM (mean BCVA 57.8 letters) versus no HRM (mean BCVA 65.4 letters), yielding a mean difference of 7.6 letters (95% confidence interval [CI], 2.3−13.0; $P = 0.005$ on a t test), which was highly statistically significant.

In the subset of 75 eyes with undefined HRM at baseline, well-defined HRM developed in 40 eyes by M12, whereas the morphology in 33 eyes improved to a stage where no HRM was detectable. The difference in BCVA outcome at M12 between these 2 groups after adjustment for baseline BCVA was +1.1 letters in favor of eyes with no HRM, but this was not statistically significant (95% CI, −3.7 to 6.0; $P = 0.65$).

The cross-sectional regression models at baseline and M12 yielded similar effect estimates. In the baseline and M12 model, each 1000-μm increase in thickness (model estimate, −0.0099; 95% CI, 0.0191−0.0017) resulted in a BCVA worsening by 10 letters. For HRM width, a 10- letter worsening was found for each 1600-μm increase (model estimate, −0.0060; CI, 0.0082−0.0037), and the M12 model showed a 10-letter worsening for 1100 μm of width. By examining the longitudinal changes from baseline to M12, the change in HRM thickness did not have an effect on change in BCVA. The change in HRM width had a highly significant impact: each 1000-μm reduction in HRM width yielded approximately 4 letters of improvement in BCVA.

Changes in OCT Features

Frequencies of specific OCT features at baseline and M12 by nAMD subtype are summarized in Supplemental Table S2 (available at www.ophthalmologyretina.org). At baseline, bridge arch−shaped SRD was most commonly seen in type 2 CNV and mixed CNV, and was persistent in 3.3% of eyes (n = 5) at M12. Bridge arch−shaped SRD was almost never observed in the absence of type 2 CNV and was strongly associated with scar at both baseline (chi-square, 24.7; $P < 0.001$) and M12 (chi-square, 13.6; $P < 0.001$).

At baseline, outer retinal tubulation was absent and only 2 eyes had CMD. At M12, outer retinal tubulation and CMD increased to 8.7% (n = 13) and 10.0% (n = 15) of eyes, respectively.

Table 2. Proportion of Eyes by Hyperreflective Material Morphology and Location at Baseline and after Anti-VEGF Therapy

	Baseline	Month 1	Month 3	Month 6	Month 12
HRM morphology					
No HRM	22 (14.6%)	52 (34.6%)	60 (40.0%)	57 (38.0%)	63 (42.0%)
Well-defined HRM	53 (35.3%)	92 (61.3%)	88 (58.7%)	84 (56.0%)	85 (56.7%)
Undefined HRM	75 (50.0%)	6 (4.0%)	2 (1.3%)	9 (6.0%)	2 (1.3%)
HRM location					
SR HRM	100 (66.7%)	17 (11.3%)	16 (10.7%)	13 (8.7%)	6 (6.0%)
SR and IR HRM	18 (12.0%)	1 (0.7%)	0 (0.0%)	2 (1.3%)	0 (0.0%)
Sub-RPE HRM	7 (4.7%)	65 (43.3%)	72 (48.0%)	71 (47.3%)	75 (50.0%)
SR and sub-RPE HRM	3 (2.0%)	6 (4.0%)	2 (1.3%)	6 (4.0%)	3 (2.0%)

HRM = hyperreflctive material; IR = intraretinal; SR = subretinal; sub-RPE = subretinal pigment eipithelial; VEGF = vascular endothelial growth factor.
Total number of eyes included = 150.

Table 3. Baseline and Month 12 Hyperreflective Material Thickness and Width by Angiographic Subtype of Neovascular Age-Related Macular Degeneration

CNV	Baseline HRM Thickness (μm)	M12 HRM Thickness (μm)	P Value	Baseline HRM Width (μm)	M12 HRM Width (μm)	P Value
Type 1 (n = 40)	130±158	59±138	0.034	946±904	399±628	<0.001
Type 2 (n = 41)	228±168	145±70	0.006	1778±861	1258±937	<0.001
Type 3 (n = 31)	280±406	27±53	0.001	927±787	340±633	0.002
Mixed (n =27)	176±63	107±65	<0.001	1679±778	1297±910	0.03
PCV (n = 11)	165±165	102±141	0.08	1233±1083	499±593	0.009
Total (n = 150)	199±230	88±104	<0.001	1322±934	791±885	<0.001

CNV = choroidal neovascularization; HRM = hyperreflective material; M12 = month 12; PCV = polypoidal choroidal vasculopathy.
P values were determined using paired *t* test.

Changes in the RPE band over time are shown in Supplemental Table S3 (available at www.ophthalmologyretina.org). At baseline in a proportion of eyes with type 2 and mixed CNV, the hyperreflective band of the RPE formed 2 distinct layers at the margins of the area of HRM, which we referred to as RPE splitting. In addition, a well-delineated hyperreflective line was present overlying the area of HRM in approximately half of the eyes with type 2 CNV and mixed CNV. By contrast, both these features were infrequent in the other nAMD subtypes. After initiation of anti-VEGF treatment, the split RPE bands frequently enveloped the reducing HRM. At M12, the hyperreflective line above HRM was rarely observed, and RPE splitting with enveloping of the residual HRM was present in 46.3% (19/41) of eyes presenting with type 2 CNV. None of these features was statistically significantly associated with BCVA outcomes, but the hyperreflective line overlying the HRM and the RPE splitting at baseline were strongly associated with macular scarring at baseline and M12 (Supplemental Table S4, available at www.ophthalmologyretina.org). Of note, RPE splitting 1 month after treatment was strongly associated with the presence of nonfibrotic scar at M12 (Supplemental Table S4).

Macular Scar and Macular Atrophy

A significant change in the proportion of eyes exhibiting fibrotic scar, nonfibrotic scar, and MA occurred from baseline to M12 (Table 5). No relationship was found between the drug administered, dosing regimens, and scar evolution.

At baseline, 40.0% (60/150) of eyes were graded as exhibiting scars (fibrotic or nonfibrotic), which were most common in type 2 and mixed CNVs. At M12, the majority of eyes with type 2 CNV (97.6%, 40/41) and mixed CNV (85.2%, 23/27) exhibited macular scar. At baseline macular scar was less common in the pure type 1, type 3 and PCV nAMD subsets, but by M12 macular scar had developed in around one half of eyes with pure type 1 CNV and around one third of eyes with type 3 CNV.

Compared with eyes with no HRM, the presence of any HRM at baseline resulted in macular scar at M12 (chi square, 31.27; $P < 0.001$, Supplemental Table S5, available at www.ophthalmologyretina.org). At M12, the sub-RPE location of HRM (almost all of which was classified as exhibiting defined borders) was strongly associated with the presence of macular scar (chi-square, 82.1; $P < 0.001$).

Logistic regression was performed to identify risk factors for scar at M12, and the final parsimonious model included only the following baseline variables: any scar, fibrin, lipid, and HRM thickness and width. The coefficient of HRM width in this model was 0.0012, indicating that an HRM width of 700 μm results in a doubling of the odds of progression to any scar (fibrotic or nonfibrotic). Variables excluded by this model were blood, HRM type, EZ disruption, ELM disruption, and number of treatments. The ordinal regression model, which tested the relationship between HRM at baseline and scar (fibrotic and nonfibrotic scar) at M12, showed that both thickness and width of HRM influenced development of fibrotic scar but not nonfibrotic scar (Table 6).

The general linear models that examined the impact of fibrotic and nonfibrotic scars on M12 BCVA are shown in Table 7. Fibrotic scarring resulted in statistically significantly worse visual outcome ($P < 0.001$), and although nonfibrotic scarring also resulted in numerically worse vision, this did not reach statistical significance (Table 7).

MA, which was present in only 14.0% (21/150) of eyes at baseline, increased to 60.0% (90/150) of eyes at M12. Type 1 and type 3 CNV accounted for the majority of eyes with MA at M12 (Table 5). Baseline HRM presence or subtype did not significantly influence the development of MA.

Ordinal regression analysis showed that risk factors for progression to MA were the presence of reticular psuedodrusen and HRM thickness (Table 8).

The general linear model with adjustment for baseline BCVA showed that eyes that developed MA had a worse BCVA outcome at M12 compared with eyes without MA (Table 9). On examining MA severity at M12 and BCVA at M12 using homogeneous subsets, the categories of no MA and mild MA were not different in BCVA. The 2 categories of moderate or severe MA had a worse BCVA outcome.

Discussion

In this study, we systematically graded the changes at the macula after anti-VEGF therapy using multimodal imaging and described a constellation of previously unreported features in OCT hyperreflectivity, their temporal evolution, and relationships to the nAMD subtypes. We characterized the OCT features associated with the resolution of undefined HRM and the onset of defined HRM, features that we had reported on previously.[9] We also explored relationships between the 2 types of HRM and evolution of macular scar, atrophy, and visual outcome at M12.

Use of high-resolution OCT has made it possible to observe noninvasively the sequence of morphologic changes at the Bruch membrane, RPE, and the photoreceptor interface occurring during anti-VEGF treatment. In this study we observed the presence of a distinct hyperreflective line above the HRM and splitting of the bands attributable to the RPE. Because the hyperreflective line above the HRM had no definite continuity with any of the other OCT retinal bands, the nature of this OCT finding is unclear.
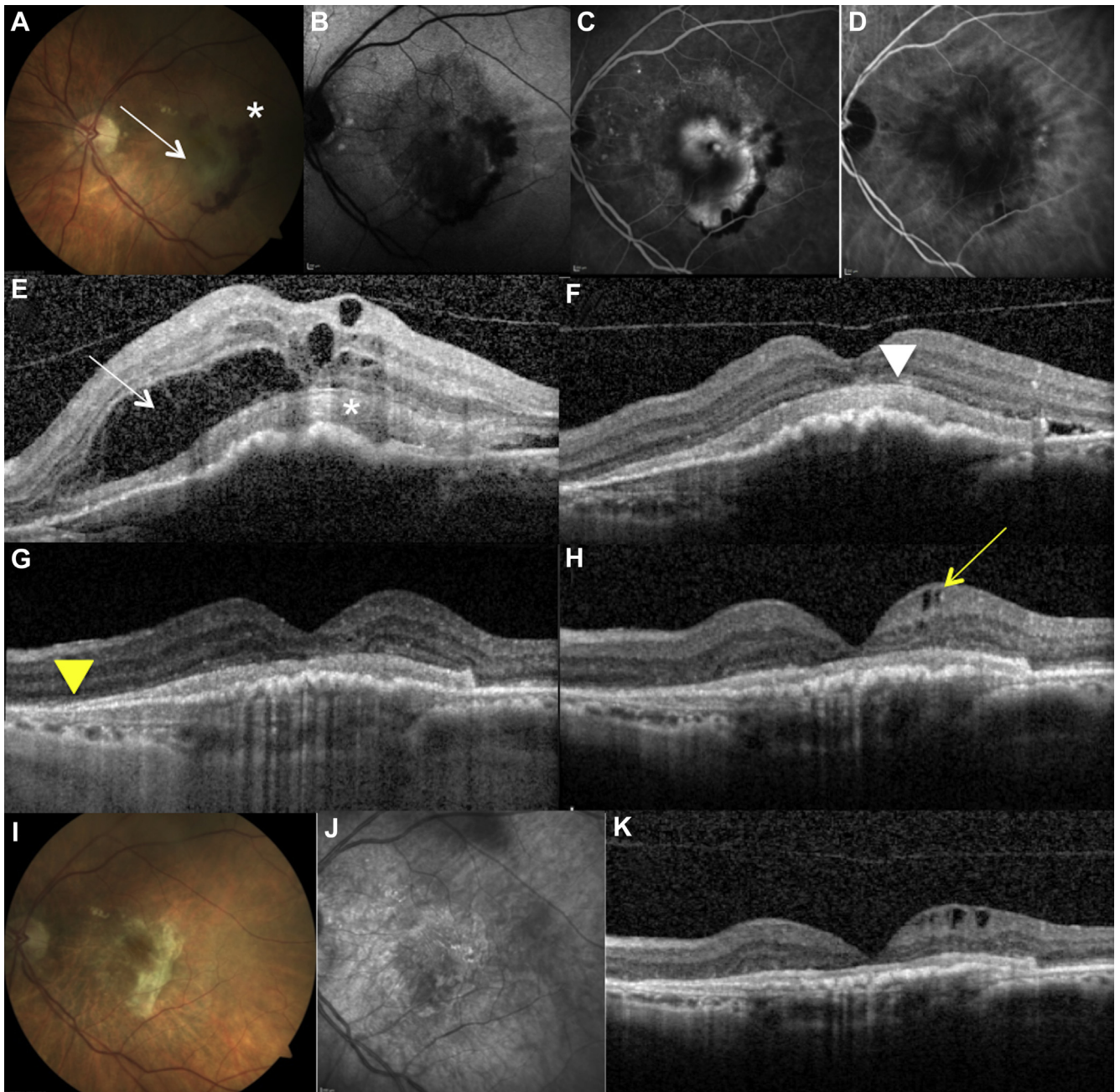
Figure 1. Multimodal imaging of neovascular age-related macular degeneration (nAMD) of the left eye. Best-corrected visual acuity (BCVA) at presentation is 58 ETDRS letters. Baseline images include color fundus photograph (CFP) (**A**), fundus autofluorescence (**B**), representative frames of the fluorescein angiogram (FA) (**C**), and indocyanine green angiogram (ICGA) (**D**). CFP reveals fibrin (*arrow* in **A**) and hemorrhage (*asterisk*). Fluorescein angiography (**C**) shows a clearly delineated area of hyperfluorescence and ICGA. **D**, a diffuse staining plaque. The baseline OCT scan (**E**) shows a well-defined hyperreflective material (HRM) (*asterisk*) with a bridge arch–shaped serous retinal detachment (SRD) (*arrow*). One month after treatment (**F**), there is resolution of the bridge arch–shaped SRD and the hyperreflective line is visible above the HRM (*arrowhead*). At month 3 (**G**) and month 6 (**H**), the retinal pigment epithelium (RPE) band (*yellow arrowhead* in **G**) is seen enveloping the reducing HRM and a few retinal cysts are observed (*yellow arrow* in **H**). Twelve months after treatment with CFP (**I**), a fibrotic scar is seen, and near-infrared reflectance imaging (**J**) showed concomitant presence of macular atrophy; the corresponding OCT scan (**K**) reveals diffuse thinning of the retina and a thin, well-defined subretinal hyperreflective band with additional bands of hyperreflectivity on both the inner and outer surfaces, which is continuous with the RPE layer at the edges of the lesion. Final BCVA is 40 ETDRS letters.

The splitting of the RPE bands, while noted even before treatment, became more marked and sometimes more extensive with complete envelopment of the HRM. We therefore speculate that reactive hyperplasia of the RPE results in envelopment of any residual HRM that most likely represents the treated CNV complex, thus leading to
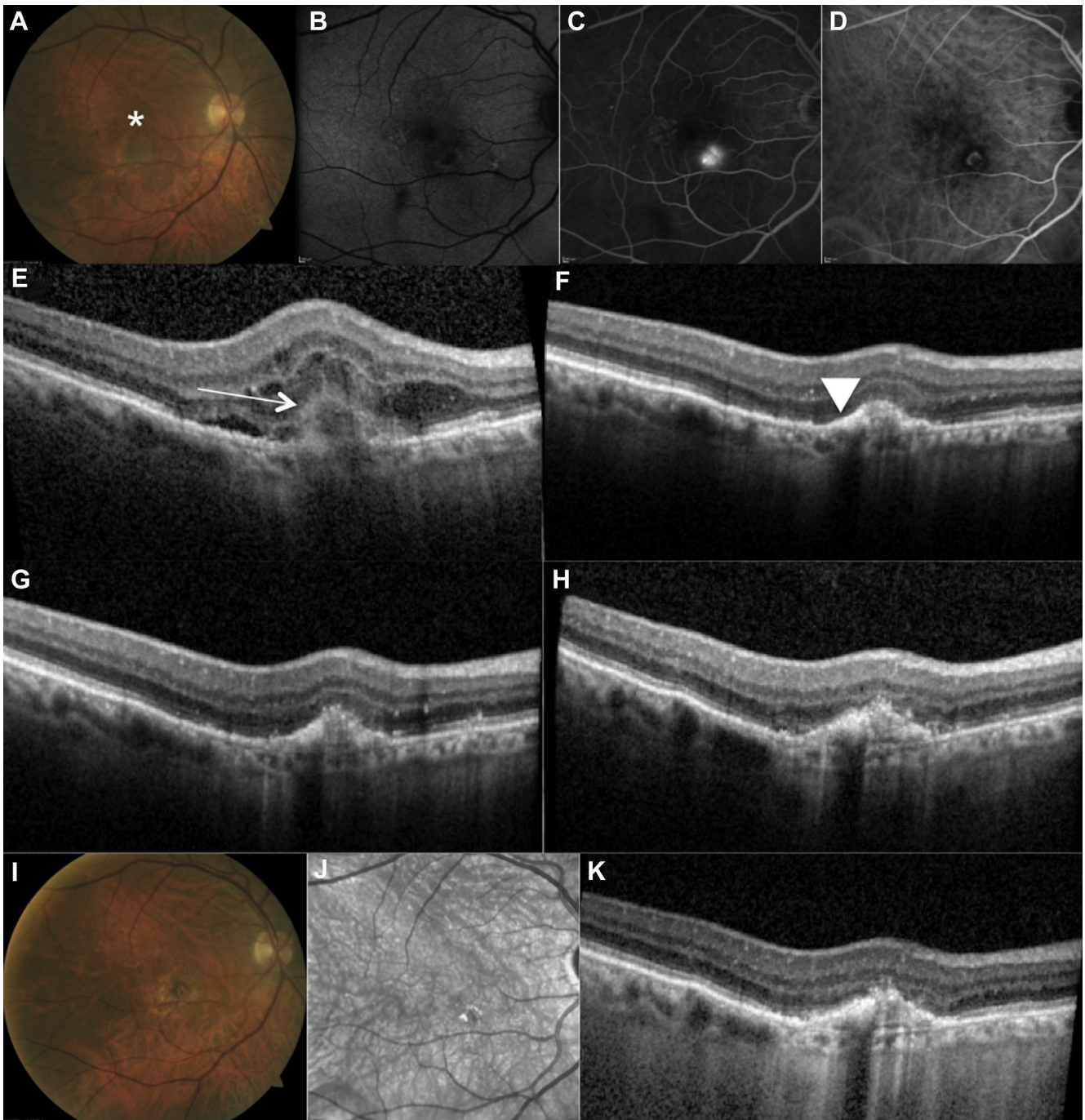
Figure 2. Multimodal imaging of neovascular age-related macular degeneration (nAMD) of the right eye. Best-corrected visual acuity (BCVA) at presentation is 78 ETDRS letters. Baseline images include color fundus photograph (CFP) (**A**), fundus autofluorescence (**B**), representative frames of the fluorescein angiogram (FA) (**C**), and indocyanine green angiogram (ICGA) (**D**). CFP (**A**) reveals a fibrinous exudative neovascular lesion (*asterisk*). FA (**C**) shows a clearly delineated area of classic choroidal neovascularization (CNV), ICGA features are consistent with a type 2 CNV (**D**). The baseline OCT scan (**E**) shows a subretinal undefined hyperreflective material (HRM) (*arrow*) with subretinal and intraretinal fluid. One month after treatment, OCT scan (**F**) shows a reducing HRM with well-defined margins. The inner margin of the HRM has become indistinguishable from the band of retinal pigment epithelium hyperreflectivity (*arrowhead*). The HRM also extends along its outer margins into the sub-RPE compartment. Subsequent OCT scans at month 3 (**G**) and month 6 (**H**) show HRM with the residual subretinal material exhibiting undefined margins. At month 12, CFP (**I**) and near-infrared reflectance imaging (**J**) show a nonfibrotic scar with good integrity of outer retinal bands on OCT (**K**). Final BCVA is 80 ETDRS letters.

recompartmentalization to a sub-RPE location.[9] In support of this theory, Schütze et al[22] recently described ring-shaped accumulations of depolarizing material at the RPE level surrounding the CNV lesion on polarization-sensitive OCT after anti-VEGF treatment in eyes with nAMD. They also attributed these findings to a reactive response at the

Table 4. Baseline and Month 12 Best-Corrected Visual Acuity and Hyperreflective Material Thickness and Width by HRM Type at Baseline

Baseline HRM Type	Baseline BCVA	M12 BCVA	Baseline HRM Thickness (μm)	M12 HRM Thickness (μm)	Baseline HRM Width (μm)	M12 HRM width (μm)
Absent (n = 22)	68.1±9.2	66.1±14.6	0	8±36	0	62±292
Undefined (n = 75)	58.2±12.4	64.4±13	262±289	74±78	1442±747	583±650
Well-defined (n = 53)	52.4±14.4	54±19	192±99	140±127	1702±894	1386±980

BCVA = best-corrected visual acuity; HRM = hyperreflective material; M12 = month 12.
BCVA is reported in ETDRS letters.

borders of a regressing CNV lesion, possibly induced by anti-VEGF therapy. More recently Dolz-Marco et al[19] described the envelopment of the neovascular hyperreflective lesion by the RPE in a small set of patients presenting with type 2 CNVs. They interpreted these findings as a regression of the type 2 into a type 1 CNV.[19]

In a previous study, Charafeddin et al[23] found that a decrease in HRM thickness and volume after treatment correlates with an improvement in VA at M12. In our model, when we included both HRM thickness and width, only the latter had a highly significant impact on BCVA improvement at M12. We interpret our findings as indicating that reductions in width likely represent complete resolution of undefined HRM at the edges of the lesion, with restoration of function in those regions of the retina. Although changes in thickness do correlate with better BCVA, they are also strongly correlated with a change in width; the latter explains a greater proportion of the variance in BCVA outcomes.

HRM has a heterogeneous composition in the treatment-naïve state. We observed interesting relationships between type of HRM and macular scar evolution at M12.

Eyes with no HRM at baseline were least likely to develop a macular scar. Eyes with defined HRM had the highest risk of scarring, whereas those with undefined HRM had a lower risk. In this context, our findings are consistent of those of CATT, in which subretinal HRM was shown to be a predictive marker for scar.[16] However, our data go beyond those of CATT, as we differentiated

between undefined HRM and well-defined HRM and, in addition, located HRM by OCT tissue layers. A high proportion of eyes with undefined HRM at baseline showed complete resolution of this OCT feature after initiation of treatment with an anti-VEGF. In those eyes in which undefined HRM at baseline was replaced with a more defined HRM over time, this change correlated with the onset of scar as detected by color image grading. The risk of developing moderate or severe fibrotic scar by M12 was double in eyes with well-defined HRM (35.8%, 19/53) compared with undefined HRM at baseline (14.6%, 11/75). We speculate that undefined HRM has a high content of fibrin and inflammatory infiltrates, whereas well-defined HRM represents formed neovascular complexes and/or preexisting fibrous elements and thus is more likely to progress to overt scar over time. The well-defined HRM observed in the treatment-naive state and the evolving defined HRM in the posttreatment phase are indistinguishable in terms of their textural characteristics on OCT. These findings suggest that (1) well-defined HRM that is present before treatment is preexisting scar tissue and (2) in some eyes undefined HRM converts into scar tissue. We therefore believe this is the most likely scenario, although we cannot rule out that newly well-defined HRM in the posttreatment phase represents a unique disease process secondary to exposure to anti-VEGF in a subset of eyes.

Regardless of the temporal evolution of the scar, we suggest the use of the term *macular scar* rather than *SR scar* because the scar extends across the SR space, the RPE, and

Table 5. Proportion of Eyes Exhibiting Scar (Fibrotic and Nonfibrotic) and Macular Atrophy at Baseline and Month 12 by Choroidal Neovascularization Subtype

CNV Subtype	Bsl Scar Fibrotic	M12 Scar Fibrotic	P Value	Bsl Scar Nonfibrotic	M12 Scar Nonfibrotic	P Value	Bsl MA	M12 MA	P Value
Type 1 (n = 40)	5.0% (2/40)	20.0% (8/40)	0.07	20.0% (8/40)	32.5% (13/40)	0.18	15.0% (6/40)	65.0% (26/40)	0.001
Type 2 (n = 41)	29.3% (12/41)	41.5% (17/41)	0.06	39.0% (16/41)	56.1% (23/41)	0.07	9.7% (4/41)	36.6% (15/41)	<0.001
Type 3 (n = 31)	0.0% (0/31)	12.9% (4/31)	NA	6.4% (2/31)	22.6% (7/31)	0.13	12.9% (4/31)	87.1% (27/31)	<0.001
Mixed (n = 27)	29.6% (8/27)	37.0% (10/27)	0.69	37.0% (10/27)	48.1% (13/27)	0.55	25.9% (7/27)	59.2% (16/27)	0.004
PCV (n = 11)	9.1% (1/11)	18.2% (2/11)	1.00	0.0% (0/11)	9.1% (1/11)	NA	0.0% (0/11)	45.4% (5/11)	NA
Total (n = 150)	15.3% (23/150)	27.3% (41/150)	<0.001	24.6% (37/150)	38.0% (57/150)	0.001	14.0% (21/150)	60.0% (90/150)	<0.001
P value	0.005	0.088		0.043	0.006		0.89	0.001	

Bsl = baseline; CNV = choroidal neovascularization; M12 = month 12; MA = macular atrophy; NA = not applicable; PCV = polypoidal choroidal vasculopathy.
The difference in proportions of eyes with fibrotic scars, nonfibrotic scars, and MA at baseline and M12 across CNV subtypes were tested using analysis of variance P values shown at the bottom of each column. The change in proportions of eyes exhibiting fibrotic scars, nonfibrotic scars, and MA between baseline and M12 were cross-tabulated and tested for significance using the McNemar exact test (P values in the rows for each feature of interest).

Table 6. Ordinal Regression Showing Influence of Hyperreflective Material Variables on Development of Fibrotic and Nonfibrotic Macular Scars

Outcome	Variable	Estimate	95% CI	P Value	Pseudo R-Square
Fibrotic scar	HRM thickness	0.0027	0.0011–0.0042	<0.001	0.436
	HRM width	0.0008	0.0003–0.0012	0.002	
Nonfibrotic scar	HRM thickness	−0.0004	−0.0022–0.0014	0.67	0.167
	HRM width	0.0001	−0.0005–0.0008	0.65	

CI = confidence interval; HRM = hyperreflective material.

the inner layers of the choroid. We also contend that the hyperreflective band on the inner aspect of the HRM and splitting of the RPE band may be considered as early OCT biomarkers for retinal scar evolution.

In this study, the prevalence of markers of established degeneration, such as outer retinal tubulation and CMD,[20,21] was low. Our patients had treatment-naïve nAMD, and they responded well to structured and regular anti-VEGF therapy during year 1; this is likely to have limited the presence of degenerative change that is more typical of long-standing disease. We observed that the bridge arch–shaped SRD was commonly encountered in treatment-naïve eyes with type 2 and mixed CNV and correlated with the presence of macular scar, and we confirm this finding as a potential biomarker for retinal scar evolution.[12] A plausible explanation for the bridge arch–shaped SRD development is that fibrin strands may promote adhesions between the sensory retina and the CNV–RPE fibrotic complex, leading to the compartmentalization of the SRD.[12]

While the pathogenic sequence of macular fibrosis in nAMD is still not completely understood, it is generally

Table 7. General Linear Model to Assess Impact of Scar at Month 12 on Visual Acuity at Month 12*

Type of Scar	BCVA Point Estimate	95% CI
Fibrotic		
Absent (n = 109)	62.5	60.3–64.6
Mild scar (n = 10)	65.0	57.9–72.2
Moderate (n = 24)	58.3	53.7–63.0
Severe (n = 7)	43.4	34.3–52.4
Nonfibrotic		
Absent (n = 93)	60.4	58.0–62.8
Barely visible (n = 14)	64.2	57.8–70.5
Mild (n = 28)	63.7	59.3–68.2
Moderate (n = 10)	60.6	53.1–68.2
Severe (n = 5)	49.3	38.7–59.9

BCVA = best-corrected visual acuity; CI = confidence interval.
BCVA is reported in ETDRS letters.
*The model showed that fibrotic scar had a statistically significant (P = 0.001) influence on BCVA with decreasing point estimates in the moderate and severe scar groups compared with eyes with absent or mild severity of fibrotic scar. The confidence limits are wide for the most severe group, as the number of eyes within this category was small. For nonfibrotic scar, BCVA was similar between the severity groups, except for the most severe category, where the point estimate was lower but failed to reach statistical significance (P = 0.129) with the confidence limits just overlapping with the other categories.

Table 8. Ordinal Regression Showing Baseline Variables Influencing Development of Macular Atrophy

Outcome	Variable	Estimate	95% CI	P Value
Macular atrophy	HRM thickness	0.0015	0.0002–0.0028	0.028
	RPD	0.80	0.146–1.45	0.017

CI = confidence interval; HRM = hyperreflective material; RPD = reticular pseudodrusen.
Psuedo R-square is 0.312.

assumed that it is the result of complex tissue repair mechanisms, consisting of sequences such as angiogenesis, formation of granulation tissue, and remodeling by connective tissue.[24] Leucocyte exudation from the highly permeable new vessels appears to play a key role in scar formation by initiating the inflammation process, stimulating glial proliferation, and ultimately generating retinal fibrosis.[25]

In a recent study, Lechner et al[26] showed higher plasma levels of complement C3a, C4a, and C5a in nAMD patients with macular fibrosis compared with nAMD patients without fibrosis and controls, suggesting that higher levels of systemic complement activation may increase the risk of macular fibrosis in patients with nAMD. Of note, the levels of these complement factors were increased in patients with type 1 and type 2 CNV but not in patients with type 3 CNV and PCV.[26] These data support the findings in this study in which there was a lower prevalence of macular scar in type 3 CNV and PCVs that tended to show MA instead.

As atrophy seen in exudative disease may be different from geographic atrophy that develops in the complete absence of exudative disease, we preferred to use the term *macular atrophy* to reflect the former.[4] MA is potentially an anatomic determinant of long-term visual outcome over the course of anti-VEGF treatment in eyes with nAMD.[3,4] In our study, eyes with MA had worse outcome in terms of BCVA at M12. Reticular pseudodrusen and thinner HRM at baseline were predictive factors for MA development. A thicker HRM at M12 appeared protective against MA. In our cohort, subretinal HRM was thickest in eyes with type 2

Table 9. General Linear Model to Assess Impact of Macular Atrophy at Month 12 on Visual Acuity at Month 12*

Macular Atrophy	BCVA Point Estimate	95% CI
None (n = 60)	62.7	59.8–65.6
Barely visible (n = 21)	66.2	61.3–71.1
Mild (n = 34)	62.5	58.7–66.3
Moderate (n = 26)	56.2	51.8–60.6
Severe (n = 9)	46.4	38.9–53.9

BCVA = best-corrected visual acuity; CI = confidence interval; GLM = general linear model; MA = macular atrophy.
BCVA is reported in ETDRS letters.
*The GLM for MA was statistically significant (P < 0.001) and shows a decreasing level of BCVA in the moderate and severe groups compared with eyes with absent or very mild macular atrophy.

CNV, and this category has been linked to lower rates of MA development.[27,28] We did not find a correlation between the number of injections administered and the risk of MA. This finding support results from recent studies that have used multimodal imaging to assess MA.[28,29] However, it remains difficult to determine whether MA onset and/or progression is linked to the anti-VEGF treatment or is simply the result of the progressive nature of the neovascular lesion.[30,31] MA may also progress in the context of very low anti-VEGF injection frequency,[4] and it strikingly spares the retinal regions beyond the arcades, which are also exposed to VEGF inhibition by intravitreal agents. These observations suggest that the development and/or progression of MA occurs as a result of cumulative damage from exudative episodes over a patient's disease course.

Strengths of this study are the large cohort of patients included from a real-life clinical setting and the longitudinal and systematic grading using a multimodal imaging approach that includes novel OCT biomarkers for atrophy and fibrosis.

The retrospective nature of the study, the absence of quantitative measurements of scar and atrophy, and the absence of a new imaging modality such as OCT angiography represent the main limitations.

References

1. Wong TY, Chakravarthy U, Klein R, et al. The natural history and prognosis of neovascular age-related macular degeneration: a systematic review of the literature and meta-analysis. *Ophthalmology*. 2008;115:116−126.
2. Hogg R, Curry E, Muldrew A, et al. Identification of lesion components that influence visual function in age-related macular degeneration. *Br J Ophthalmol*. 2003;87:609−614.
3. Maguire MG, Martin DF, Ying GS, et al; Comparison of Age-Related Macular Degeneration Treatments Trials (CATT) Research Group. Five-year outcomes with anti-vascular endothelial growth factor treatment of neovascular age-related macular degeneration: the Comparison of Age-Related Macular Degeneration Treatments Trials. *Ophthalmology*. 2016;123:1751−1761.
4. Bhisitkul RB, Mendes TS, Rofagha S, et al. Macular atrophy progression and 7-year vision outcomes in subjects from the ANCHOR, MARINA, and HORIZON studies: the SEVEN-UP study. *Am J Ophthalmol*. 2015;159:915−924.
5. Sharma S, Toth CA, Daniel E, et al; Comparison of Age-related Macular Degeneration Treatments Trials Research Group. Macular morphology and visual acuity in the second year of the Comparison of Age-Related Macular Degeneration Treatments Trials. *Ophthalmology*. 2016;123:865−875.
6. Giani A, Luiselli C, Esmaili DD, et al. Spectral-domain optical coherence tomography as an indicator of fluorescein angiography leakage from choroidal neovascularization. *Invest Ophthalmol Vis Sci*. 2011;52:5579−5586.
7. Giani A, Esmaili DD, Luiselli C, et al. Displayed reflectivity of choroidal neovascular membranes by optical coherence tomography correlates with presence of leakage by fluorescein angiography. *Retina*. 2011;31:942−948.
8. Willoughby AS, Ying GS, Toth CA, et al; Comparison of Age-Related Macular Degeneration Treatments Trials Research Group. Subretinal hyperreflective material in the Comparison of Age-Related Macular Degeneration Treatments Trials. *Ophthalmology*. 2015;122:1846−1853.
9. Casalino G, Bandello F, Chakravarthy U. Changes in neovascular lesion hyperreflectivity after anti-VEGF treatment in age-related macular degeneration: an integrated multimodal imaging analysis. *Invest Ophthalmol Vis Sci*. 2016;57:288−298.
10. Jaffe GJ, Eliott D, Wells JA, et al. A phase 1 study of intravitreous e10030 in combination with ranibizumab in neovascular age-related macular degeneration. *Ophthalmology*. 2016;123:78−85.
11. Roberts P, Sugita M, Deák G, et al. Automated identification and quantification of subretinal fibrosis in neovascular age-related macular degeneration using polarization-sensitive OCT. *Invest Ophthalmol Vis Sci*. 2016;57:1699−1705.
12. Fajnkuchen F, Cohen SY, Thay N, et al. Bridge arch-shaped serous retinal detachment in age-related macular degeneration. *Retina*. 2016;36:476−482.
13. Chakravarthy U, Harding SP, Rogers CA, et al; IVAN Study Investigators. Ranibizumab versus bevacizumab to treat neovascular age-related macular degeneration: one-year findings from the IVAN randomized trial. *Ophthalmology*. 2012;119:1399−1411.
14. Heier JS, Brown DM, Chong V, et al. Intravitreal aflibercept (VEGF trap-eye) in wet age-related macular degeneration. *Ophthalmology*. 2012;119:2537−2548.
15. Freund KB, Zweifel SA, Engelbert MR. Do we need a new classification for choroidal neovascularization in age-related macular degeneration? *Retina*. 2010;30:1333−1349.
16. Daniel E, Toth CA, Grunwald JE, et al. Risk of scar in the comparison of age-related macular degeneration treatments trials. *Ophthalmology*. 2014;121:656−666.
17. Staurenghi G, Sadda S, Chakravarthy U; International Nomenclature for Optical Coherence Tomography (IN·OCT) Panel. Proposed lexicon for anatomic landmarks in normal posterior segment spectral-domain optical coherence tomography: the IN·OCT consensus. *Ophthalmology*. 2014;121:1572−1578.
18. Zhou Q, Daniel E, Maguire MG, et al. Pseudodrusen and incidence of late age-related macular degeneration in fellow eyes in the Comparison of Age-Related Macular Degeneration Treatments Trials. *Ophthalmology*. 2016;123:1530−1540.
19. Dolz-Marco R, Phasukkijwatana N, Sarraf D, Freund KB. Regression of type 2 neovascularization into a type 1 pattern after intravitreal anti-vascular endothelial growth factor therapy for neovascular age-related macular degeneration. *Retina*. 2017;37:222−233.
20. Zweifel SA, Engelbert M, Laud K, et al. Outer retinal tubulation: a novel optical coherence tomography finding. *Arch Ophthalmol*. 2009;127:1596−1602.
21. Querques G, Coscas F, Forte R, et al. Cystoid macular degeneration in exudative age-related macular degeneration. *Am J Ophthalmol*. 2011;152:100−107.
22. Schütze C, Wedl M, Baumann B, et al. Progression of retinal pigment epithelial atrophy in antiangiogenic therapy of neovascular age-related macular degeneration. *Am J Ophthalmol*. 2015;159:1100−1114.
23. Charafeddin W, Nittala MG, Oregon A, Sadda SR. Relationship between subretinal hyperreflective material reflectivity and volume in patients with neovascular age-related macular degeneration following anti-vascular endothelial growth factor treatment. *Ophthalmic Surg Lasers Imaging Retina*. 2015;46:523−530.
24. Friedlander M. Fibrosis and diseases of the eye. *J Clin Invest*. 2007;117:576−586.

25. Jo YJ, Sonoda KH, Oshima Y, et al. Establishment of a new animal model of focal subretinal fibrosis that resembles disciform lesion in advanced age-related macular degeneration. *Invest Ophthalmol Vis Sci*. 2011;52:6089−6095.

26. Lechner J, Chen M, Hogg RE, et al. Higher plasma levels of complement C3a, C4a and C5a increase the risk of subretinal fibrosis in neovascular age-related macular degeneration: Complement activation in AMD. *Immun Ageing*. 2016;13:4.

27. Thavikulwat AT, Jacobs-El N, Kim JS, et al. Evolution of geographic atrophy in participants treated with ranibizumab for neovascular age-related macular degeneration. *Ophthalmology Retina*. 2017;1:34−41.

28. Abdelfattah NS, Al-Sheikh M, Pitetta S, et al; Treat-and-Extend Age-Related Macular Degeneration Study Group. Macular atrophy in neovascular age-related macular degeneration with monthly versus treat-and-extend ranibizumab: findings from the TREX-AMD Trial. *Ophthalmology*. 2017;124:215−223.

29. Munk MR, Ceklic L, Ebneter A, et al. Macular atrophy in patients with long-term anti-VEGF treatment for neovascular age-related macular degeneration. *Acta Ophthalmol*. 2016;94:e757−e764.

30. Grunwald JE, Daniel E, Huang J, et al; CATT Research Group. Risk of geographic atrophy in the Comparison of Age-Related Macular Degeneration Treatments Trials. *Ophthalmology*. 2014;121:150−161.

31. Chakravarthy U, Harding SP, Rogers CA, et al; IVAN study investigators. Alternative treatments to inhibit VEGF in age-related choroidal neovascularisation: 2-year findings of the IVAN randomised controlled trial. *Lancet*. 2013;382:1258−1267.

Footnotes and Financial Disclosures

[1] Ophthalmology Macular Service, Belfast Health and Social Care Trust and Centre for Population Health, Queen's University Belfast, Belfast, United Kingdom.

[2] Department of Ophthalmology, San Raffaele Scientific Institute, Vita-Salute University, Milan, Italy.

Abbreviations and Acronyms:

AMD = age-related macular degeneration; **BCVA** = best-corrected visual acuity; **CATT** = Comparison of Age-related macular degeneration Treatments Trials; **CMD** = cystoid macular degeneration; **CNV** = choroidal neovascularization; **ELM** = external limiting membrane; **ETDRS** = Early Treatment Diabetic Retinopathy Study; **EZ** = ellipsoid zone; **FA** = fluorescein angiography; **HRM** = hyperreflective material; **ICGA** = indocyanine green angiography; **IR** = intraretinal; **M12** = month 12; **MA** = macular atrophy; **MC** = multicolour; **nAMD** = neovascular AMD; **PCV** = polypoidal choroidal vasculopathy; **RPE** = retinal pigment epithelium; **SR** = subretinal; **SRD** = serous retinal detachment; **sub-RPE** = subretinal pigment epithelial; **VA** = visual acuity; **VEGF** = vascular endothelial growth factor.

Correspondence:
Usha Chakravarthy, MD, PhD, Professor, Centre for Experimental Medicine, School of Medicine, Dentistry and Biomedical Sciences, Queen's University Belfast, Institute of Clinical Science, Block A Grosvenor Road, Belfast, Northern Ireland BT126BA, United Kingdom. E-mail: U.Chakravarthy@qub.ac.uk.